References

Baranne, A., et al., 1996, *A&A Suppl Ser*
119,1.

Butler, R.P., et al. 1996, *PASP* **108**, 500.

Hatzes, A.P. & Cochran, W.D. 1993, *ApJ*
413, 339.

Hatzes, A.P. & Cochran, W.D. 1994a, *ApJ*
422, 366.

Hatzes, A.P. & Cochran, W.D. 1994b, *ApJ*
432, 763.

Hatzes, A.P. & Cochran, W.D. 1998, *MNRAS*
293, 469.

Kaufer, A., et al. 1999, *The Messenger* **95**, 8.

Larson, A. et al. 1993, *PASP* **105**, 825.

Lambert, D.L. 1987, *ApJS* **65**, 255.

Merline, W.J. 1996, ASP Conf. Ser. **135**, p.
208.

Pasquini, L., Pallavicini, R. Pakull, M. 1988,
A&A **191**, 266.

Pasquini, L. 1992, *A&A* **266**, 347.

von der Lühe, O., Solanki, S., Reinheimer,
Th. 1996, in IAU Symp. 176, *Stellar
Surface Structure* 147–163. Walker,
G.A.H., Yang, S., Campbell, B., and Irwin,
A.W. 1989, *ApJL* **343**, L21.

Crowded Field Photometry with the VLT: the Case of the Peculiar Globular Cluster NGC 6712

*F. PARESCE[1], G. DE MARCHI[2], G. ANDREUZZI[3], R. BUONANNO[3], F. FERRARO[4],
B. PALTRINIERI[3], L. PULONE[3]*

[1]*European Southern Observatory, Garching, Germany*
[2]*European Space Agency, STScI, Baltimore, USA*
[3]*Osservatorio Astronomico di Roma, Rome, Italy*
[4]*Osservatorio Astronomico di Bologna, Bologna, Italy*

1. Introduction

The Hubble Space Telescope opened up the exciting possibility of carrying out very deep, high-precision stellar photometry in very crowded fields such as those routinely encountered in the core of dense stellar clusters and galaxies. This capability has allowed, for example, the reliable detection of stars all the way down to the bottom of the main sequence (MS) at the centre of nearby globular clusters (GC) six or seven magnitudes below the turn-off (TO) and well into the brown dwarf substellar region of nearby star-forming regions and of resolving the evolved stellar populations in nearby dwarf galaxies. Enormous progress in our understanding of the age, distance, star formation rates, and mass functions of a large sample of stellar populations has been a direct result of the last ten years of HST.

The advent of the VLT with wide-field optical and IR cameras such as FORS and ISAAC present us with a golden opportunity to push further our quest for good quality photometry of faint sources in crowded fields. The potential of very good and stable seeing coupled with the huge collecting area of an 8-m diameter telescope with wide field and broad spectral coverage detectors certainly rivals and even surpasses, in principle, even the exceptional HST capability in this endeavour. In order to test these capabilities in practice, our group proposed to study in depth a particularly interesting example of a crowded stellar environment namely the GC NGC 6712.

We report here the preliminary results of our study of this cluster using FORS1 and UT1 obtained with 12 hours of observations during Period 63. We emphasise those aspects of the

study that best illuminate the performance of this instrument combination for crowded field photometry that might be of interest to anyone contemplating doing this sort of work with the VLT in the future. Results from a preliminary study of this object using the VLT Test Camera during the UT1 Science Verification period were reported in De Marchi et al. (1999).

2. VLT Observations of NGC 6712

NGC 6712 (= 18^h 53^m 04.3 , = –08° 42 21.5) is a relatively metal poor, small and sparse GC ([Fe/H] = –1.01 and concentration ratio c = 0.9; Harris 1996) located in the midst of a rich star field at the centre of the Scutum cloud (Sandage 1965), which
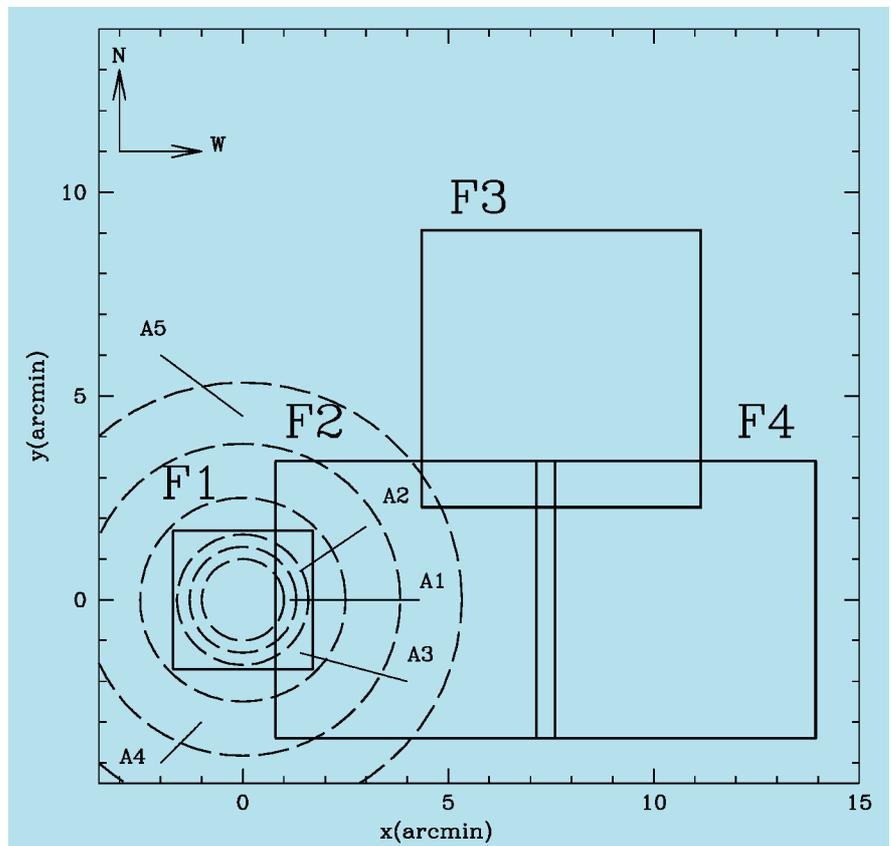

Figure 1: Locations of the four FORS1 fields on NGC 6712. The centre of the cluster is located at the origin of the co-ordinate system.

Figure 2: VLT-FORS1 high-resolution image (180s exposure) of the core of NGC6712 in the R band (field F1). The size of the image is 3.4′ × 3.4′. North is up and East to the left.

is one of the highest surface-brightness regions with high space-density gradients of the Milky Way (Karaali 1978). Its Galactic orbit forces it to penetrate deeply into the bulge. With a perigalactic distance smaller than 300 pc, this cluster ventures so frequently and so deeply into the Galactic bulge (Dauphole et al. 1996) that it is likely to have undergone severe tidal shocking during the numerous encounters with both the disk and the bulge during its lifetime. The latest Galactic plane crossing could have happened as late as $4 \cdot 10^6$ year ago (Cudworth 1988), which is much less than its half-mass relaxation time of 1 Gyr (Harris 1996). It is precisely on this basis that Takahashi & Portegies Zwart (2000) have suggested that NGC 6712 may have lost

99% of its mass during its lifetime. If true, this implies that NGC 6712 was originally one of the most massive clusters in the Galaxy.

There are two peculiarities of this seemingly inconsequential cluster that point to its being now only a pale reflection of its former glory. The first is the presence in the core of the well-known high luminosity X-ray source (X1850-086) with an optical counterpart (Anderson et al. 1993). This is unexpected for such a loose cluster because most clusters with such sources tend to have a much higher central concentration. The second is a clear and continuous drop of its global mass function (MF) with decreasing mass starting already at the TO and continuing down to the observation limit at ~ 0.5 $M_\odot$

(Vesperini & Heggie 1997). For all the other clusters surveyed so far with HST in this mass range, the global MF increases steadily with decreasing mass (Paresce & De Marchi 2000).

NGC 6712, therefore, could hold the key to a better understanding of the observable effects of tidal interactions, and especially to learning more about the mechanisms leading to the dissolution of GC in the Galaxy and about the possible variation of the cluster IMF with time. The specific objectives of our study were twofold: (1) to obtain a more precise LF of the MS below the TO at various distances from the centre, so as to evaluate the possible effects of mass segregation on the derived MF and to sample more of the cluster at or near the tidal radius to see whether or

not one could detect an excess of low-mass stars ejected from the interior and still lightly bound to the cluster; (2) to study the evolved population above the turn-off in greater detail than has been possible heretofore in order to determine more precisely the hot star population characteristics and the cluster age and distance.

For this, we obtained deep images of 5 fields in the V and R bands, four of which are located as shown in Figure 1. The fifth field, used as a control field (field F0), is located 42′ N of the cluster centre and was imaged using the standard FORS1 resolution of 0.2″/pixel.
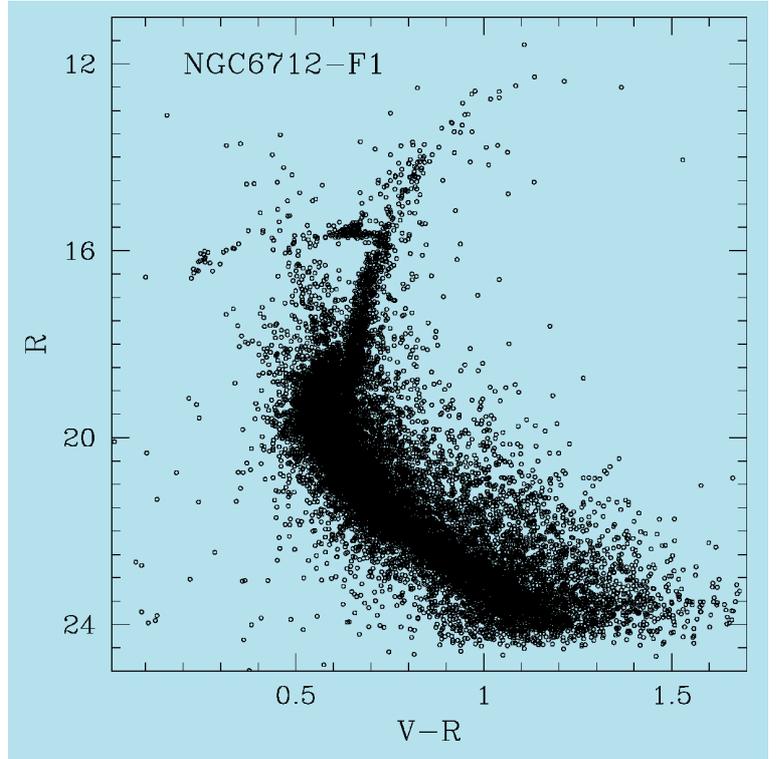
Because the level of crowding varies considerably from the core of the cluster out to its periphery, our observations were carried out according to the following strategy: the fields covering the external regions of the cluster were imaged at standard resolution (SR, plate-scale 0.2″/pixel) with 4 900-s exposures and cover an area of 46.2 arcmin square each (6.8′ × 6.8′); they are located respectively 5′ W (field F2), 8′ NW (field F3) and 11′ W (field F4) of the centre of the cluster; to improve the photometry in the central regions, where the level of crowding is particularly high, we have covered it with images taken in the high resolution mode of FORS1 (HR, plate-scale 0.1″/pixel) with 4 180-s exposures, with a field 3.4′ × 3.4′ in size (field F1). To ensure a homogeneous calibration and to transform the co-ordinates into a common local system from the centre of the cluster out to the more external regions, each field has been selected so as to overlap with at least a neighbouring one.

In order to study the evolved part of the CMD above the turn-off where the effects of saturation in the bright stars would otherwise seriously compromise the photometric accuracy, five 10-s B-, V-, R-band exposures, five 120-s U-band exposures were taken for each field. An additional 700-s HO exposure was obtained only in the central field F1. The long exposure (180 s) R-band image of this latter field covering the core of the cluster obtained with 0.3″ seeing is shown in Figure 2. This image gives a good idea of the level of crowding encountered in this situation. All the data were taken in good seeing conditions ranging from 0.3″ to 0.7″ in service mode. Images taken during the best seeing conditions in high resolution mode compare quite favourably with existing archive short exposure images taken with the WFPC2 camera on HST outside the core.

3. Data Reduction

Except for a small subset of the R-band images, we have adopted the reduced and calibrated (i.e. bias-subtracted and flat-fielded) data as provided by the standard ESO-VLT pipeline.

Figure 3: Colour-magnitude diagram of the stars in field F1 (core) of NGC 6712

Some of the raw R-band data, however, had not been processed through the automated pipeline, and for them we had to run standard IRAF routines following the same recipe employed in the ESO-VLT pipeline. Subsequent data reduction and analysis was done using standard IRAF photometry routines *(digiphot.daophot)*.

Since our goal was to reliably detect the faintest object in these images, for each field and filter we first created a mean frame using all available applicable frames and then ran the standard *digiphot.daofind* routine on the average images so obtained to locate stars. Typical values of the PSF-FWHM are 0.3″ and 0.7″, respectively at high and low resolution. Although, in principle, we could have also averaged images in different filters, the presence of bad columns in the R-band frames (usually due to heavily saturated pixels and spikes of the bright stars) suggested not to follow this approach. With a detection threshold set in the V and R bands typically at 3–5 σ above the local average background level, we obtained two independent co-ordinate lists for each field (one per filter), which we then fed to the PSF-fitting routine *allstar* to measure the instrumental magnitude of each object in each filter. We found that a Moffat function gave the best representation of the shape of the PSF, both at high and low resolution.

The positions of the identified objects in each mean R and V-band image were matched to one another, so as to obtain a final catalogue containing only the positions and magnitudes of the stars common to both filters.

Objects lying in overlapping regions between two adjacent fields were used to determine the transformations between instrumental magnitudes and to translate *local* frame co-ordinates to a *common* co-ordinate system, with origin at the cluster centre. Typically, about one hundred stars in each overlapping region were used to derive such transformations. Only linear transformations were used to match star measurements, with all magnitudes being referred to those of the high resolution field (F1). For stars in the overlapping region, multiple magnitude measurements were averaged using appropriate weights (which take into account the photometric quality of each field). At the end of this procedure, a homogeneous set of instrumental magnitudes, colour and positions (referred to field F1) were obtained for a total of 106,092 stars, in F1, F2, F3 and F4.

Instrumental (F1) magnitudes were finally transformed to the standard Johnson system, using the stars in common with the bright portion of the CMD which has been properly calibrated using ten photometric standard stars in selected areas PG1528, PG2213, PG2331 (Landolt 1992). Since we have repeated exposures in each filter, the internal accuracy of our photometry has been estimated from the rms frame-to-frame scatter of the instrumental magnitudes. The resulting mean photometric errors are very small (σ < 0.05) over the whole bright magnitude range (R = 13 to 21) covered by our short exposure observations in all the filters while they vary from 0.05 to 0.1 mag in the deep exposure observations of the MS below the TO. Figure 3 shows the total CMD of the central region of NGC 6712 (field F1). The figure is obtained by merging the deep (180-s long expo-
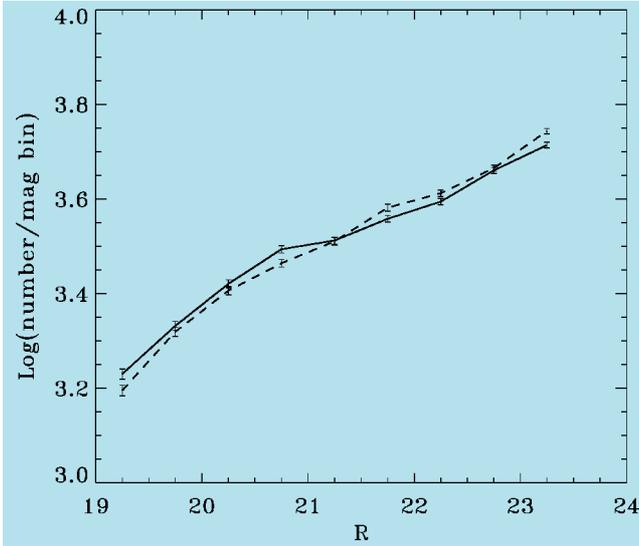
Figure 4: Luminosity functions measured in fields F0 (dashed line) and F3 (solid line).

sure) and the bright (10-s exposure) data covering the core of the cluster.

Especially for the deep images probing the faint end of the cluster MS, correction for incompleteness clearly becomes of critical importance. The correction depends on the level of crowding in the observed fields and, therefore, on their location with respect to the cluster centre. In particular, an insufficient or inappropriate correction for crowding will result in the distortion of the stellar LF with a preferential loss of fainter stars and a relative increase of bright and spurious objects. In our case, crowding is not the only source of incompleteness: the distribution in luminosity of the stars is also modified by the large number of hot pixels and bad columns affecting the original images.

To correct our photometry for incompleteness, we ran artificial star tests on both sets of frames (V and R) independently, so as to be able to estimate the overall completeness of our final CMD. First, we applied the artificial star test to the mean R-band images: artificial stars in each given 0.5 magnitude bin were added randomly to the frames, making sure not to exceed a few per cent ($\simeq$ 10%) of the total number of stars actually present in that bin so as to avoid a significant enhancement of image crowding. We then added an equal number of stars at the same positions in the V-band frames and with a magnitude such that they would fall on the cluster MS. It should be noted that we made the assumption that all artificial stars were to lie on the MS since our intent was to verify the photometric completeness of MS stars. This procedure was repeated for all the bins of each field's CMD in both filters. To obtain a robust result, we simulated more than 200,000 stars in 250 artificial images for each field.

All pairs of V and R frames obtained in this way were then subjected to

the same analysis used for the original frames, with the result being a catalogue of matching objects, each characterised by a position and a pair of V and R-band magnitudes. Each of these 250 catalogues (one per artificial pair of images) was compared with the catalogue of input artificial stars: an artificial star was considered detected only when its final position and magnitudes were found to coincide with the input catalogue within x, y $\leq$ 1.5 pixel, mag $\leq$ 0.3. This approach allowed us to build a map showing how photometric incompleteness varies with position in our frames. Completeness reaches the 50% level at V $\simeq$ R $\simeq$ 23 at $r = 70$ from the core, for example. Inside this point, the level of crowding and the large ensuing incompleteness would have resulted in a poor determination of the LF. Moreover, we did not include a region between $r = 116$ and 150 because the level of crowding there is too high for the low resolution of the FORS1 camera at 0.2 /pixel and a standard seeing quality of FWHM $\simeq$ 0.6 .

Finally, inspection of the CMD presented in Figure 3 shows that the field contamination is particularly severe in the region of NGC 6712. A reliable determination of the physical characteristics and especially of the LF of NGC 6712 requires that we account for the

contamination caused by field stars. We have dealt with this correction in a statistical way by using the comparison field FO, for which we have produced a CMD and assessed photometric incompleteness precisely as we did for all other fields. When it comes to measuring the LF – our final goal – we subtract from the stars found in a given magnitude on the cluster CMD the objects detected in the same magnitude bin in an area of equal size on the FO field. Clearly, both numbers are corrected for their respective photometric incompleteness before doing the subtraction.

4. Data Analysis and Interpretation

By applying the statistical field star subtraction described above, we discovered that stars located in fields F3 and F4 can be considered as belonging to the field because all the objects in the CMD of these fields are statistically compatible with being field stars. We show this in Figure 4, where we plot the R-band LF, corrected for incompleteness, as measured in fields F3 and FO (respectively solid and dashed line). The absence of any significant trend or systematic departures of one function with respect to the other (within 2) confirms that there are no residual cluster stars at distances greater than ~ 5 from the cluster centre.

A plot of the radial density profile determined from our sample of stars brighter than V $\simeq$ 20 shown in Figure 5 confirms this result. The thick dashed line marks a typical King-type profile with core radius $r_c = 55$ and tidal radius $r_t = 5.1$, superposed to a plateau of field stars. A tidal radius of ~ 5 is fully consistent with our finding of a statistically null cluster in Fields F3 and F4 and implies that it will always be very difficult to detect an excess of cluster low mass stars at or beyond the tidal radius ejected from the interior and still lightly bound to the cluster due to the very severe field contamination against which these faint stars have to be detected.

As a result of these findings, we considered all stars lying in F3 and F4 as field stars, thus improving the statistical sample of the field, and redefined the decontamination procedure above using as comparison field the whole catalogue
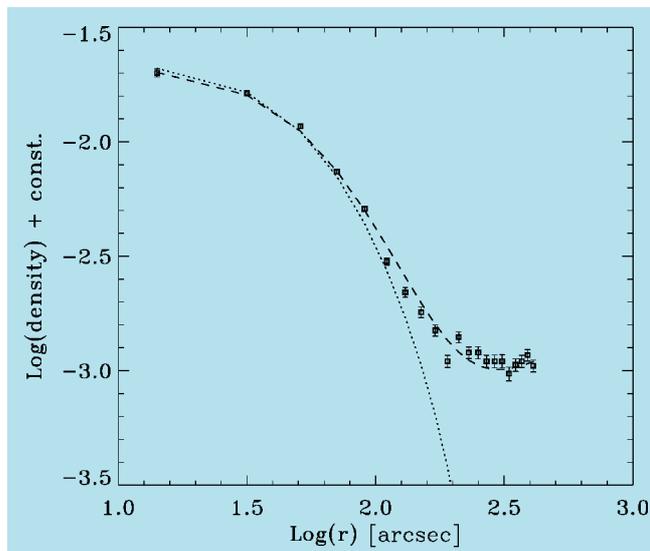

Figure 5: Surface density profile of ~ 0.75 $M_\odot$ stars. The thin line shows a King-type profile with $r_c = 60''$ and $r_t = 300''$, whereas the thick dashed line shows the superposition of the latter on a plateau of field stars of uniform surface density.
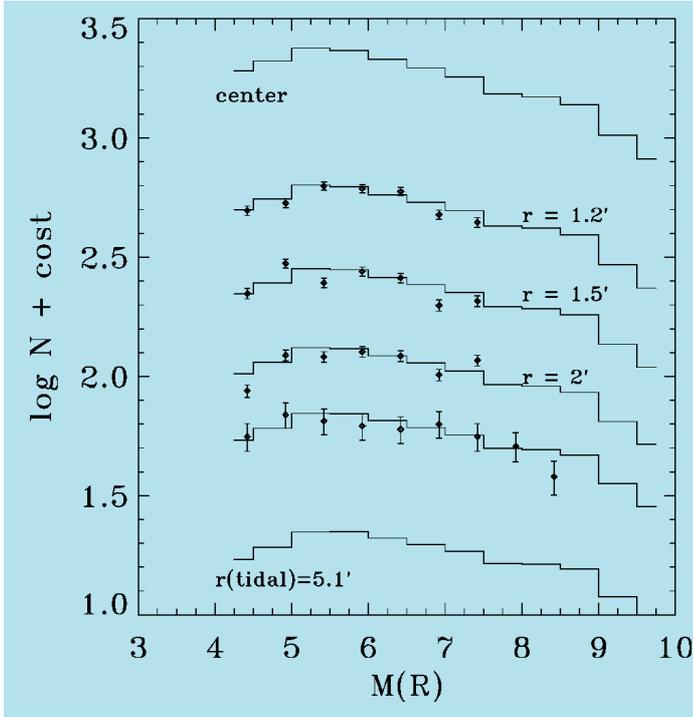
for F3, F4 and F0 (r 5). This result also strongly implies that the field around NGC 6712 is relatively uniform at our required level of accuracy thereby fully justifying our confidence that the field contamination at the position of the cluster is properly accounted for. We, therefore, regarded only the F1 and F2 fields as containing cluster stars. Because of the richness of our sample, we investigated the variation of the LF as a function of distance on a scale smaller than the typical size of a frame.
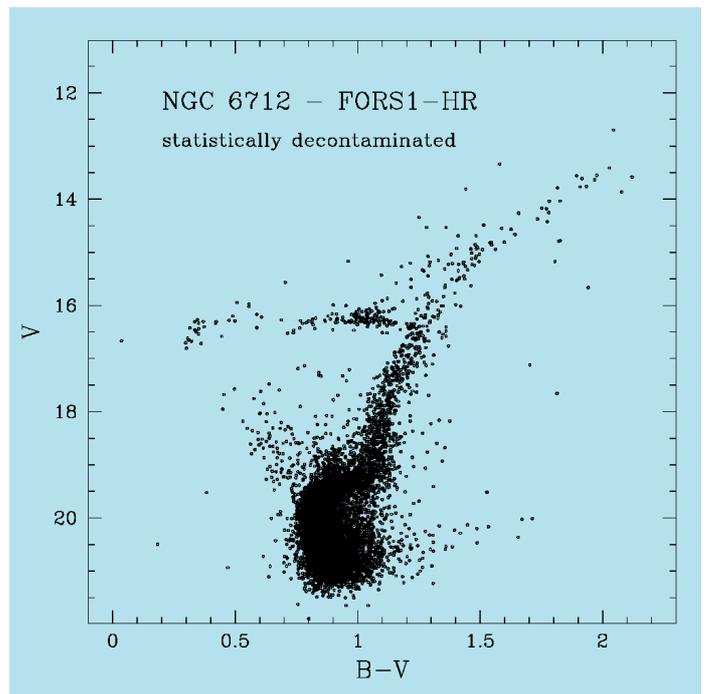
The LF determined in annuli centred at 1.2 , 1.5 , 2 and 2.25 from the centre and of average thickness ~ 0.1 are shown in Figure 6 together with the theoretical expectations of a Michie-King multi-mass model at these distances and, for comparison, at the centre and at the tidal radius. The best fit is obtained with a power-law global MF with an index of $\simeq$ 0.9. The key result here, then, is that the global MF of NGC 6712 is indeed an inverted function, i.e. one that decreases with decreasing mass below ~ 0.8 $M_\odot$. Although all clusters whose LF has been studied in the core show an inverted local MF there (as a result of mass segregation: see e.g. Paresce, De Marchi & Jedrzejewski 1995; King, Sosin & Cool 1995; De Marchi & Paresce 1996), NGC 6712 is *the only known cluster so far* to feature an inverted MF on a global scale.

The field star decontamination procedure was also applied to each of the CMDs resulting from the brief exposures in the central Field 1. Figure 7 shows the (V, $B - V$) CMD statistically decontaminated for this field. Here the result is quite good as the statistical decontamination successfully removes

most of the field stars and the cluster sequences appear clearly well defined. In particular, the large population of blue straggler stars (BSS) is clearly visible together with a few blue objects present in the very central region of NGC 6712 and lying outside the main loci defined by the cluster stars. These include three faint and one bright blue stars. The peculiar blue colour of these stars is confirmed by the (U, $U - B$) CMD (Figure 8) where they are plotted as filled triangles.

The bright star (#9620) located roughly at the HB level but significantly bluer than the bluest HB stars is the most UV-bright object in the field. Its

position in the CMD closely resembles that of the UV-bright post-AGB star found in M3 (vZ1128, see Buonanno et al. 1994). Such objects are indeed very rare in GC: only a few post-AGB stars have been found in GC due to their short evolutionary lifetime of ~ 10^5 yr (only 0.5 Post-AGB stars are expected to be found in a typical ~ 10^5 $L_\odot$ cluster). In order to check whether the position of this star is consistent with the hypothesis that it is a post-AGB star, we performed a qualitative comparison with theoretical models. A ~ 12.5 Gyr isochrone with appropriate metallicity (Z = 0.004) from Bertelli et al. 1994 has been over-plotted in the CMD of Figure 8 as a reference. It has been shifted to fit the main loci in order to show the location of the post-AGB track and the subsequent cooling sequence. As can be seen, the position of the UV-bright star in the CMD nicely agrees with that predicted by the theoretical cooling track.

Two out of the three faint UV-excess stars (namely #10261 and #9774) are located within the cluster core. Star #9774 is star *S* identified by Anderson et al. (1993) as the optical counterpart to the known luminous low-mass X-ray binary (LMXB). Its position is only ~ 1 away from the X-ray source, in agreement with Anderson et al. (1993). Our observations confirm that it is the bluest object within ~ 15 of the X-ray source s nominal position, and for this reason it remains the best candidate to be the optical counterpart to the LMXB. Star #10261 is the brightest object among the three faint UV sources in Figure 8. Moreover, it is the only object showing a clearcut H emission in the core of NGC 6712. The other two UV-excess stars have *normal* colour (($H\alpha - R$) > – 0.1), and thus they are fully compatible,
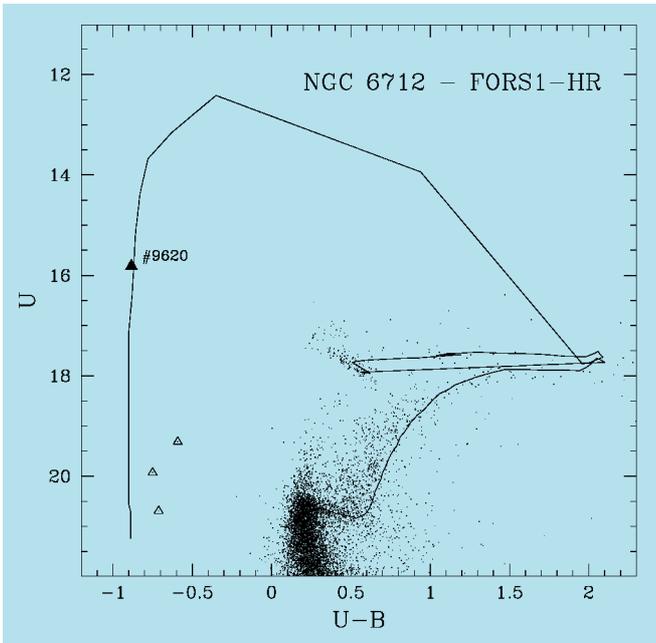
Figure 8: U, U − B CMD of NGC 6712 from FORS1-high-resolution im-
ages. The bright blue object #9620 is plotted as a large filled triangle.
The three faint UV stars are plotted as open triangles. An isochrone
from Bertelli et al. (1994) is also plotted for reference.

within the errors, with the ($H\alpha - R$) colour of *normal* cluster MS stars.

UV-excess and H emission together-er with X-ray emission are characteristic signatures of interacting binaries (IB). In fact, when a binary system contains a compact object (like a neutron star or a white dwarf) and a close enough secondary, mass transfer can take place: the streaming gas, its impact zone on the compact object and the presence of an accretion disk can give such systems observational signatures which make them stand out above ordinary cluster stars. These signatures include X-ray emission, significant radiation in the ultraviolet, H emission lines, X-ray emission, etc. In particular, Cool et al. (1995) have shown the efficiency of the H-emission technique in pinpointing candidate IB among the *normal* GC population. For this reason, we can consider star #10261 as a very promising IB. Interestingly enough, the new IB discovered by us in the core of NGC 6712 is located only a few arcsec away from star #9774, the optical counterpart to the LMXB.

Thus NGC 6712 turns out to harbour in its core two unrelated IB systems a few arcsec apart. This fact, coupled with a large BSS population and an inverted mass function, indicates an unusual level of dynamical activity for a GC of such a moderate density, suggesting again that, at some early epoch, NGC 6712 was much more massive and concentrated than now, and its interaction with the Galaxy is driving it towards dissolution.

This result demonstrates the huge potential of the VLT for exploring the IB population in moderate-density GC. For

this reason, we intend to further exploit the sensitivity of FORS1 at UT1 to search for H- and UV-excess from IB in a set of GC with moderate central density. The project as a whole will finally shed light on the formation and evolution of IB (and their progeny) in GC.

5. Lessons Learned

Several lessons were learned from this exercise concerning the use of the VLT for crowded-field photometry. Some of them were already alluded to in the text but we summarise them here for clarity. The photometric accuracy and completeness level depend crucially on several factors: level of crowding especially of the bright stars, pixel size and seeing. Obviously, a delicate balance has to be found between these parameters which determines the exposure time to limit the effect of saturation and the ultimate limiting magnitude reached in each filter. In general, we found that:

1. because of the high density of bright objects, only very short exposures taken with the high-resolution (HR) mode of FORS1 and seeing better than 0.3 yields acceptable results in the core of a GC with more than ~ 1 star/arcsec^2. Consequently, only the evolved part of the CMD of the core of a cluster can be studied with the FORS1+UT combination. For deeper images in the core, HST and, possibly, the CONICA+NAOS combination for small fields would be preferred.

2. The FORS1+UT combination and seeing better than 0.5 (routinely obtained at Paranal) is the ideal combination to search for relatively faint objects (U > 20) like the IB in the central region of moderate-density GC (log ρ < 3) with large core radius ($r_c > 1$). Our observations show that the VLT can be used as a complementary instrument to HST in efficiently searching for peculiar objects in the relatively large cores of moderate density clusters. The HST/WFPC2 combination due to its peculiar shape and small field of view is not well adapted to image clusters with large core radii.

3. Outside the core beyond about twice the half mass radius where crowding is still high but less of an is-

sue, the Standard Resolution (SR) mode of FORS1 is useful only if the seeing is very good (< 0.5) and exposures are kept short enough to prevent severe saturation of the brightest red giants (about 200 s for NGC 6712 in the *R* band). If this is not the case, the high-resolution (HR) mode yields the best results even for moderate seeing (< 0.8).

4. In any kind of crowded field, if the seeing is good (< 0.6), the SR mode should be avoided if field size is not an issue. The SR mode is really useful only for sparsely crowded fields like those in an open cluster or in the periphery of a GC.

5. Registering dithered images is very useful in correcting for hot pixels.

6. The data-quality flag that is activated at the level of 3% saturated pixels should be deactivated to allow the image to pass through the pipeline processing so as not to waste time re-analysing the image afterwards (the pipeline software is not available to users).

Notwithstanding these difficulties, our observations of NGC 6712 have clearly shown that the VLT can be quite competitive with HST even in the case of crowded fields provided the proper combination of camera resolution, seeing and exposure time is adopted. In this case, the large collecting area of the VLT allows good photometric accuracy associated with more efficient and flexible scheduling than possible with HST.

References

Anderson, S., Margon, B., Deutsch, E., Downes, R. 1993, *AJ* **106**, 1049.

Bertelli, G., Bressan, A., Chiosi, C., Fagotto, F., Nasi, E. 1994, *A&AS*, **106**, 275.

Buonanno, R., Corsi, C., Buzzoni, A., Cacciari, C., Ferraro, F., Fusi Pecci, F. 1994, *A&A*, **290**, 69.

Cool, A., Grindlay, J., Cohn, H., Lugger, P. Slavin, S. 1995, *ApJ*, **439**, 695.

Cudworth, K.M. 1988, *AJ* **96**, 105.

Dauphole, B., Geffret, M., Colin, J., Ducourant, C., Odenkirchen, M., Tucholke, H. 1996, *A&A*, **313**, 119.

De Marchi, G., Leibundgut, B., Paresce, F., Pulone, L. 1999, *AA* **343**, L9.

De Marchi, G., Paresce, F. 1996, *ApJ*, **467**, 658.

Harris W. 1996, *AJ*, **112**, 1487.

Karaali, S. 1979, *AAS*, **35**, 241.

King, I.R., Sosin, C., & Cool, A. 1995, *ApJ*, **452**, L33.

Landolt, A. 1992, *AJ*, **104**, 372.

Paresce, F., De Marchi G. 2000, *ApJ*, **543**, 870.

Paresce, F., De Marchi G., Jedrzejewski, R. 1995, *ApJ*, **442**, L57.

Sandage, A., Smith, L.L. 1966, *ApJ* **144**, 886.

Takahashi, K., Portegies Zwart, S. 2000, *ApJ*, **535**, 759.

Vesperini,E., Heggie, D. 1997 *MNRAS* **289**, 898.